# Computational insights into the agonist activity of cannabinoid receptor type-2 ligands using molecular dynamics simulation

**Vivek Kumar Yadav***

Department of Chemistry, School of Advanced Sciences and Languages, VIT Bhopal University, Bhopal 466 114, India

**Cannabinoid (CB) receptors belong to the G protein-coupled receptor (GPCR) family and were activated by endogenous, phytogenic and synthetic modulators. The CB receptors are involved in a variety of physiological processes, including appetite, pain sensation, mood, memory, etc. The potency of ligands with receptors provides the path through which the latter show agonist, antagonist, or inverse agonist behaviour. Due to the unavailability of crystal structure of CB type-2 (CB2) receptor, we used multiple template comparative homology modelling algorithms to construct 3D models for the same. We performed docking and molecular dynamics simulation study of four synthetic drugs in both cannabinoid type-1 (CB1) and CB2 receptors. These ligands show agonist activity with the CB2 receptor and activates it completely. The results are compared with the CB1 receptor. Molecular properties of the ligands, including molecular, polar and solvent-accessible surface areas, and intramolecular hydrogen bonds were evaluated using molecular dynamics simulations. Our finding demonstrates that the ligand AM-1221 shows the highest binding affinity (–12.73 k cal/mol), whereas UR-144 shows the lowest (–9.83 k cal/mol) towards the CB2 receptor. These findings should stimulate the design of ligands with distinct pharmacological properties associated with the CB2 receptor.**

**Keywords:** Agonist activity, cannabinoid receptors, induced fit docking, ligands, molecular dynamics simulations.

OWING to their unique behaviour, cannabinoids (CBs) have been the focus of extensive chemical and biological research[1]. CB receptors in mammalian tissues are expressed as either CB type-1 (CB1) or CB type-2 (CB2), as both belong to the G-protein-coupled receptor (GPCR) family. These receptors also behave as inverse agonist, which indicates that CB1 and CB2 receptors can exist in a constitutively active state. In the early 1970s, research exploring the psychotropic effects of cannabis comprised primarily of trans-Δ-9-tetrahydrocannabinol (Δ-9-THC) and in the 1980s it reached the clinics for trials. In general, CB receptors belong to the class of receptors which respond to CB drugs. *Cannabis sativa* (also known as marijuana) and its biologically active synthetic analogues such as THC belong to this class[1–3]. The significant role of CB receptors is to repress neurotransmitter release in the brain. THC is the primary psychoactive compound found in cannabis and some other plants[4,5]. Another major constituent from plants is cannabidiol (CBD), which is a non-psychoactive CB. Like tranquilizers, CBs also affect a person directly by interacting with specific receptors which are located within the central nervous system. CB1 is the central cannabinoid receptor (brain receptor), while CB2 is the peripheral cannabinoid receptor (body/immune system receptor). CB1 receptors are expressed predominantly at nerve terminals where they mediate inhibition of transmitter release, whereas CB2 receptors are found mainly on immune cells. The major difference between CB1 and CB2 receptors is in their amino acid sequence, signalling mechanism and in tissue distribution.

The structure of CB1 and CB2 consists of seven transmembrane-spanning domains, as commonly seen in GPCRs[6]. Class A GPCRs have a common topology which includes an extracellular N-terminus with a transmembrane core that is formed by a bundle of seven transmembrane $\alpha$-helices (TMH1-7), three extracellular (EC) and three intracellular (IC) loops that connect these helices, and an intracellular C-terminus[7–10]. CB2 has a glycosylated N-terminus and an intracellular C-terminus which plays a critical role inducing the receptor to become less responsive to certain ligands. Human CB2 receptor consists of approximately 360 amino acids, about 25% less compared with the CB1 receptor. The CB2 receptor is liable for anti-inflammatory and other therapeutic effects of cannabis detected in animal models[11]. Initially, it was believed that CB2 receptor was present primarily in the immune cells, but later it has been reported that the CB2 receptor is localized neuronally in distinct species. Different types of compounds mainly targeting CB2 have been discovered and show selective CB2 agonist activity[12,13]. The CB2 receptor plays a vital therapeutic role specifically with agonist JWH-015 in neurodegenerative disorders like Alzheimer's disease[14,15], as this combination debars beta-amyloid protein from human tissues[16].

Some CB ligands that show agonist activity with CB1 and CB2 receptors can interact with them with similar

*e-mail: vivek@vitbhopal.ac.in

strength. The ligand-protein binding affinity studies also suggest that CB2 agonist ligands interact with the receptor site (inside binding pocket) differently, supporting the pharmacodynamics concepts[17–20]. CB2 receptors are found in various types of inflammatory cells and immunocompetent cells. An antinocceptive response is generated in the position of inflammatory hyperalgesia and neuropathic pain due to activation of peripheral CB2 receptors[21,22]. The mechanism which governs this CB2-mediated effect is the generation of inflammatory hyperalgesia[23]. In general, it is considered that the activation of CB1 receptors is related to the central side effects, which include ataxia and catalepsy, whereas selective CB2 receptor agonist potentially treats the pain without causing side effects. In addition, CB2 receptors have novel pain-control actions. A CB2-induced cannabinoid compound can inflict hyperalgesia of diversified origins and play a vital role even in neuropathic pain[24], which are conditions often refractory to therapy.

In this study, we exclusively focus on the interaction of four synthetic illicit drugs with CB1 and CB2 receptors. According to the US Department of Health and Human Services, by grade 12, about half of the adolescents have used an illicit drug like 'marijuana' at least once[25]. On the other hand, these drugs in combination with CB receptors are effective against various immune systems and play a vital role in pain transmission and neurodegenerative disorders[26]. The four ligands used in the present study are AM-1221, AM-2232, UR-144 and JWH-015 (refs 27–30).

All of them are agonist and show higher binding affinity towards CB2 than CB1. Among these four ligands, AM-1221 has greater affinity towards CB2 due to the presence of 2-methyl and 6-nitro groups on the indole ring which makes it highly CB2-selective. Figure 1 shows the structures of these ligands along with CB2 receptor.

## Methods

### *Homology modelling and sequence alignment*

The UniProt database (http://www.uniprot.org) was used to retrieve the amino acid sequences of CB1 and CB2 receptors.

CB1 sequence (UniProt accession code: P21554): MKSILDGLADTTFRTITTDLLYVGSNDIQYEDIKGDMASKLGYFPQKFPL TSFRGSPFQEKMTAGDNPQLVPADQVNITEFYNKSLSSFKENEENIQCGE NFMDIECFMVLNPSQQLAIAVLSLTLGTFTVLENLLVLCVILHSRSLRCRP SYHFIGSLAVADLLGSVIFVYSFIDFHVFHRKDSRNVFLFKLGGVTASFTA SVGSLFLTAIDRYISIHRPLAYKRIVTRPKAVVAFCLMWTIAIVIAVLPLLGWNCEKLQSVCSDIFPHIDETYLMFWIGVTSVLLLFIVYAYMYILWKAHSH AVRMIQRGTQKSIIIHTSEDGKVQVTRPDQARMDIRLAKTLVLILVVLIIC WGPLLAIMVYDVFGKMNKLIKTVFAFCSMLCLLNSTVNPIIYALRSKDLR HAFRSMFPSCEGTAQPLDNSMGDSDCLHKHANNAASVHRAAESCIKSTV KIAKVTMSVSTDTSAEAL.

CB2 sequence (UniProt accession code: P34972): MEECWVTEIANGSKDGLDSNPMKDYMILSGPQKTAVAVLCTLLGLLSAL ENVAVLYLILSSHLRRKPSYLFIGSLAGADFLASVVFACSFVNFHVFHGVD SKAVFLLKIGSVTMTFTASVGSLLLTAIDRYLCLRYPPSYKALLTRGRALV TLGIMWVLSALVSYLPLMGWTCCPRPCSELFPLIPNDYLLSWLLFIAFLF SGIIYTYGHVLWKAHQHVASLSGHQDRQVPGMARMRLDVRLAKTLGLV LAVLLICWFPVLALMAHSLATTLSDQVKKAFAFCSMLCLINSMVNPVIYA LRSGEIRSSAHHCLAHWKKCVRGLGSEAKEEAPRSSVTETEADGKITPW PDSRDLDLSDC.

Due to lack of experimentally crystallized structure of the protein of interest, homology modelling provides a robust path to predict the correct 3D structure of proteins. Till date, there is no experimental crystal structure available for the CB receptor. Therefore we developed a homology model for CB2.

CB1 and CB2 show nearly 44% match in the entire protein sequence as well as almost 75% in the seven transmembrane regions. The homology modelling begins with template identification, alignment and model building till refinement. Once the 3D model was developed, it was rigorously validated by studying the various structural parameters and related structural quality assessment.

We used Prime[31–33] for development of the 3D model for protein and refinement followed by their validation using BioLuminate suite[34–37]. BLAST homology search which fetches the regions of local similarity between biological sequences was used to identify the best homologous

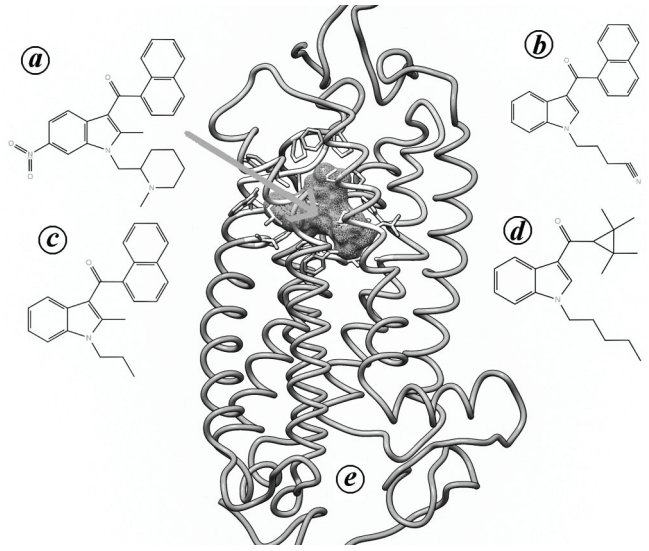


**Figure 1.** Chemical structures of small-molecule ligands. (***a***) AM-1221, (***b***) AM-2232, (***c***) JWH-015, (***d***) UR-144. (***e***) Induced fit docking ligand AM-1221 (surface mesh) in the binding pocket of cannabinoid type-2 (CB2) receptor.

experimental protein structure from the Protein Data Bank (PDB) repository[38]. BLOSUM62 similarity matrix was used to calculate the alignment score. A database protein must have at least 40% sequence identity, high resolution and the most appropriate cofactors for it to be considered as a template sequence.

We used the gap-opening penalty cost of 11.0 for the gap in sequence alignment and a 1.0 penalty score for each gap extension. BLAST homology search with an inclusion threshold of 0.005 was used for maximum of three iterations. We used the thermo-stabilized human A2A receptor (PDB code: 2YDO) as a base template for the active state of CB2 (ref. 39). The crystal structure of the human CB1 receptor has been recently reported[40]. SSPro was used for prediction of secondary structure, whereas Prime STA GPCR-specific alignment was used for sequence alignment. We employed knowledge-based model building method, to construct 10 models in each run. We also used a VSGB solvation model to refine the loops with OPLS 2005 force field and their respective charges. After construction of the main chain atoms, the next target was to assign their positions accurately. This is important to identify protein–ligand interactions at the active sites and the protein–protein interactions at their contact interfaces. The in-home built 3D model was then energy-minimized to remove the atomic clashes. The final refined model was evaluated for checking the angles, chirality, bond lengths, close contacts, etc. using the BioLuminate suite. One can develop a successful model based on correct template selection, the algorithm used and validation of the model.

### *Protein preparation*

We prepared the protein in the protein preparation wizard of Schrödinger before kickoff ligand-docking[41,42]. In protein preparation, the structure is typically imported from PDB and the unwanted water molecules are removed. In this wizard, the original hydrogen atoms are replaced by new ones and the bond order is adjusted to rectify the errors in the proteins. Structures with missing residues near the active site must be repaired. By adjusting the orientations and relative state of the interacting groups like ASN, GLN, TYR, THR, SER and HIS, the hydrogen bonding network was corrected. Finally, the protein structure was refined by restrained energy minimization employing OPLS 2005 force field. Figure 1 *e* shows the structure of CB2 receptor with ligand AM-1221 after docking. The crystal structure of CB1 (PDB accession code: 5XR8) was used as the template for modelling studies[40].

### *Ligand preparation*

Appropriate preparation of ligand structures is necessary for modelling/docking task. This can be achieved using the LigPrep module of Schrödinger to prepare the 3D ligands[43]. Maestro 2D sketcher was used to prepare the initial ligand structures and further converted into 3D structures to produce corresponding low-energy 3D output. We did not perform any pre-docking filtering and included all the structures. We prepared ligands with the OPLS 2005 force field and charges, and only conserved those ligands which had low-energy conformers.

### *Induced fit docking*

The receptors are not rigid in nature, whereas the standard virtual docking studies assume them to be rigid. To overcome this problem, we employed the induced fit docking method using the induced fit docking (IFD) protocol of Schrödinger for ligand docking to predict their binding mode and impact on structural changes of the receptor[44,45]. We prepared a docking receptor grid using cavities THR97, PHE100, TRP179, THR183, and MET263 for the CB1 receptor and PHE87, THR116, PHE117, ILE198 and TRP258 for the CB2 receptor[46]. Constrained minimization of the receptors was done with a root mean square deviation (RMSD) cut-off of 0.18 Å using a softened potential glide docking for each ligand. A maximum of 20 poses for each ligand was retained which needed to satisfy the criteria of Coulomb-*v*d*W* score below 100 and H-bond score less than 0.05. To get the best protein/ligand flexible binding domain, the Prime Molecular Dynamics module was used for those amino residues which fell within 5 Å of each pose. Glide redocking of each set of the protein/ligand complex was performed using GlideSP (ref. 47), with the best 20 poses within 30 kcal/mol.

### *Molecular dynamics simulations*

The final coordinates of the best-docked ligands into CB1 and CB2 receptors were selected and used in the input file for molecular dynamics simulation employing DESMOND software and using OPLS2005 force field[48–51]. We used the system-builder module of DESMOND to set-up the system and immersed the complex into the POPC membrane with neutralizing counter ions with per-equilibrated TIP3P water bath at 303 K, such that the prepared system was surrounded by a periodic box of water and extended approximately 10 Å in each direction. The RESPA integrator algorithm was employed in the numerical integration with a bonded time step of 2 ps (ref. 52). The Nose–Hoover chain thermostat method was used to control the thermostat with a relaxation time step of 1.0 ps (ref. 53). The Barostat method proposed by Martyna *et al.*[54] was employed with a relaxation time step of 2.0 ps, with isotropic molecule-based scaling to maintain constant pressure during simulation. For Lennard–Jones interactions, a cut-off of 9.0 Å was applied for the short-range Coulombic interactions and smooth particle mesh Ewald method was

**Table 1.** Details of protein family and globally conserved residue for the cannabinoid type-2 (CB2) receptor

| Query | Template PDB ID | % Identity | % Similarity | Family | E-value |
|---|---|---|---|---|---|
| CB2 | 2YDO | 26 | 46 | 7TM 1–7 Transmembrane receptor (rhodopsin family) | 1.2e–44 |

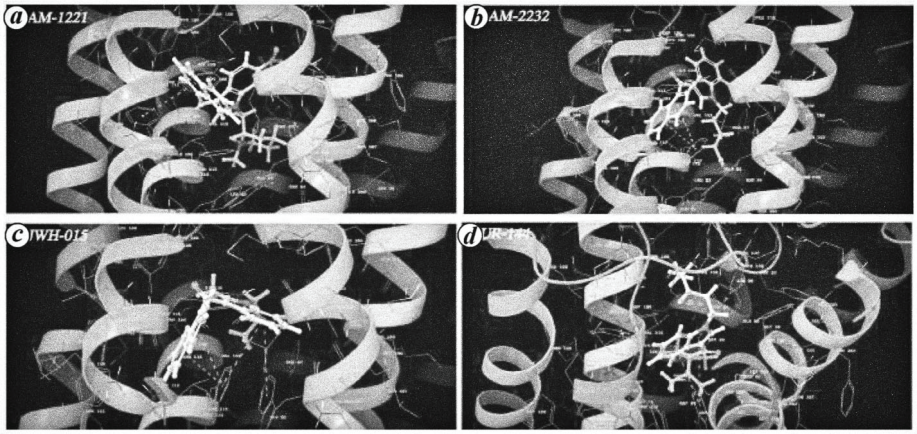


**Figure 2.** 3D structure of the ligands: (***a***) AM-1221, (***b***) AM-2232, (***c***) JWH015 and (***d***) UR-144 inside the binding pocket of the CB2 receptor. The $\pi$–$\pi$ interaction between the ligand and residues of the CB2 receptor is shown in dashed line.

used with tolerance of 1e-09 for long-range forces. The generated system was then energy-minimized for 5000 iterations. After minimization of the structure, the system underwent six relaxation steps before the molecular dynamics production step. After initial equilibration, the 100 ns production trajectories were generated using NPT ensemble for various structural and dynamical analyses. RMSD, root mean square fluctuation (RMSF) and other structural features were computed using the in-built simulation interaction method of DESMOND.

## Results and discussion

Homology modelling is a unique and transparent way to generate 3D models of proteins having significant importance in science/nature because of the large ratio between the number of known protein sequences and the number of solved proteins structure[55]. In this study, we developed ten 3D models of CB2 receptor and conserved the best residue for docking and simulations. It is recommended to check the structural closeness in the protein family and general behaviour in their structural and biological properties. Table 1 provides details of the protein family and the globally conserved residue. By defining the protein family and globally conserved residue, one gets the precise idea about the experimental 3D feature of the protein of interest. We used the template with the highest matching sequence identity with our target sequence. The IFD module of Schrödinger was used for docking of the ligands in CB receptors. We chose this module over other docking modules because in IFD, ligands induce conformational changes in the active site of proteins upon binding. Standard docking modules such as SP and XP assumes that receptors are rigid in nature but this is not the case as receptors/proteins show flexible behaviour in their shapes and binding modes while interacting with the ligands.

### *Docking results*

Figure 2 shows the docking results for all the four ligands into the CB2 receptor. In this figure the docking/binding sites are zoomed in order to explore the type the interaction that the ligands make with the surrounding residues of CB2. IFD of ligand AM-1221 into CB1 and CB2 receptors show a docking score of –13.48 and –12.729 k cal/mol respectively. For CB1 (Figure 3 *a*), residue THR201 shows direct side-chain hydrogen bonding with the ligand inside the binding pocket and makes it stable (Figure 3 *a*). The residues VAL291, PHE278, ILE290, TRP279, LEU360, LEU359, MET363, ILE362, PHE379, PHE177, CYS382, CYS386, LEU387, VAL 96 and PHE174 show hydrophobic interaction with the AM-1221 ligand inside the pocket, within the 4 Å cut-off. The residues THR197, SER199, SER 383 and SER390 also show polar interaction with the ligand. The pi–cation interaction is also found between the ligand and residues PHE200 and PHE170.

For IFD of ligand AM-1221 in the CB2 receptor, the residue VAL113 shows direct hydrogen bonding with the ligand, which makes it stable in the binding pocket. Other residues like PHE 197 and PHE 87 show $\pi$–$\pi$ interaction and $\pi$–$\pi$ stacking respectively. The ligand experiences hydrophobic interactions with nearby residue such as

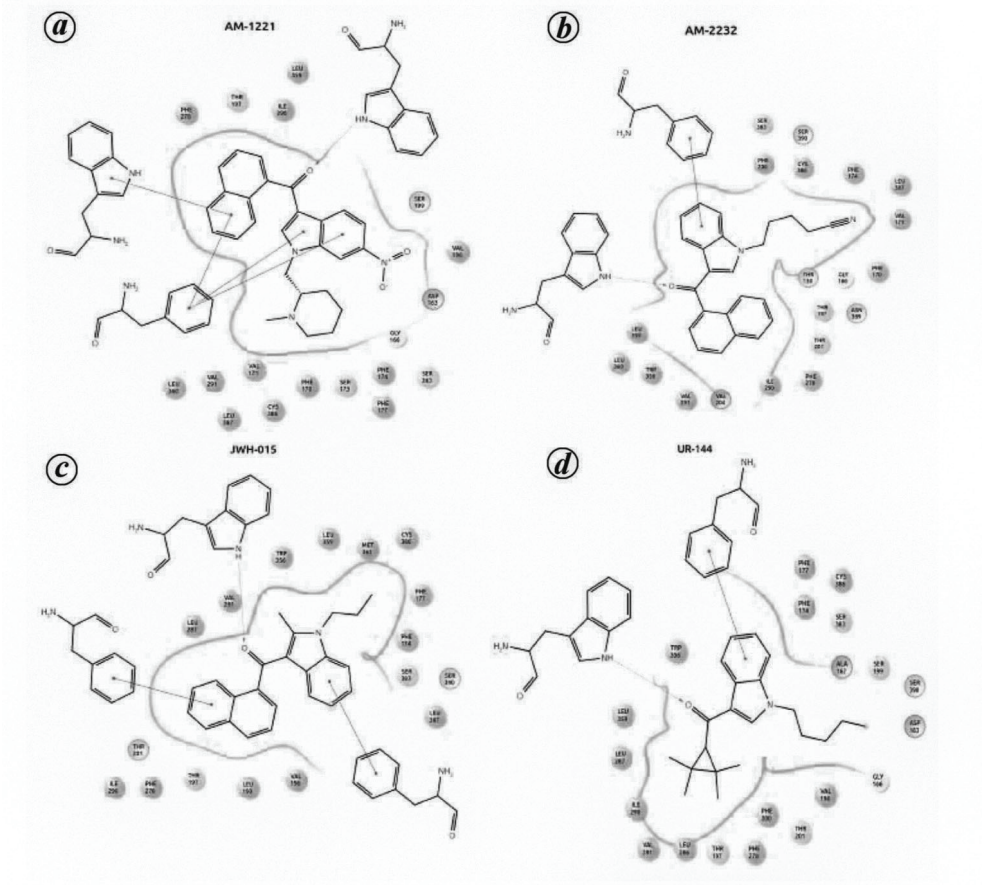


**Figure 3.** Ligand interaction diagram of (***a***) AM-1221, (***b***) AM-2232, (***c***) JWH-015 and (***d***) UR-144 with cannabinoid type-1 (CB1) receptor. The hydrophobic interaction within the 4 Å region of the ligand with the residues is shown, whereas the $\pi$–$\pi$ interaction is shown by solid line.

ALA83, PHE117, PRO178, TYR190, LEU191, TRP194 and ILE198 within the 4 Å cut-off (Figure 4 *a*). Residue ASP189 shows positive charged interaction towards the ligand. The ligand shows polar interaction with THR114, THR116, ASN188, SER193 and SER285 within the same range of cut-off. Figures 3 and 4 are ligand interaction diagrams describing the various interactions.

We performed a similar docking protocol for the AM-2232 ligand in the CB1 and CB2 receptors. The docking score was found to be –12.38 and –11.048 k cal/mol respectively. The residue TRP279 makes direct hydrogen bonding with the ligand inside the binding pocket with the oxygen atom. The residues PHE278, ILE290, VAL204, VAL291, TRP356, LEU360, LEU359, CYS386, PHE200, PHE170, PHE174, LEU387 and VAL171 show hydrophobic interaction with the ligand within the 4 Å cut-off (Figure 3 *b*). Residues SER383, ASN389, THR201, THR197, THR130 and SER390 influence polar interaction with the ligand. Residue PHE177 shows $\pi$–$\pi$ stacking with the ligand inside the binding pocket of the CB1 receptor.

This ligand also shows a stronger affinity towards the CB2 receptor, and its binding energy with the CB2 receptor is comparable with the CB1 receptor. In Figure 4 *b*, residue TRP258 shows direct hydrogen bonding with the terminal nitrogen atom of the ligand and PHE117 shows $\pi$–$\pi$ stacking with the two nearby rings of the ligand with equal strength. In the binding capsule, the ligand is well trapped with the residues PHE87, VAL121, PRO178, TYR190, TRP194, ILE198, LEU262 and MET265 with hydrophobic interaction within the 4 Å region. Some polar residues like THR114, THR116, THR118, ASN188, SER165 and SER286 help stabilize the ligand in the pocket. The ligand is approached by the negatively charged moiety ASP189. The literature and experimental results also confirm the same behaviour of the ligand with the receptor[56,57].

Another agonist subtype-selective CB ligand of interest is JWH-015. Like the other two ligands, this also helps stabilize the binding pocket of the CB2 receptor. The docking score of this ligand in the CB1 and CB2 receptor pockets is –11.86 and –10.745 k cal/mol respectively. For the CB1-JWH-015 system, the docked ligand shows direct hydrogen bonding interaction with residue TRP279 of the receptor (Figure 3 *c*). Whereas residues like ILE290, PHE278, LEU287, VAL291, MET363, TRP356, LEU359,

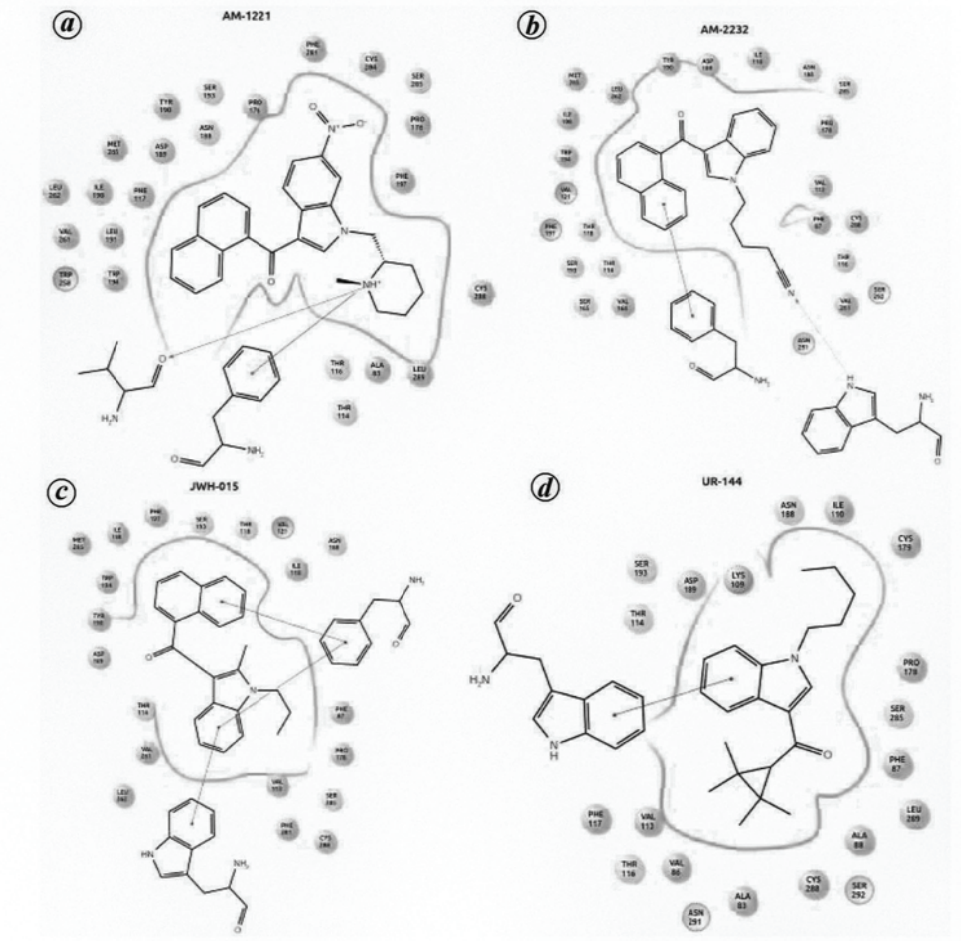


**Figure 4.** Ligand interaction diagram of (***a***) AM-1221, (***b***) AM-2232, (***c***) JWH-015 and (***d***) UR-144 with CB2 receptor. The hydrophobic interaction within the 4 Å region of the ligand with the residues are shown, whereas the $\pi$–$\pi$ interaction is shown by solid line.

CYS386, PHE174, PHE177, LEU387, VAL196 and LEU193 show hydrophobic interaction with the docked ligand. Few residues such as SER390, THR197, THR201 and SER383 show polar interaction with the ligand. Residue PHE170 shows $\pi$–$\pi$ stacking with the docked ligand.

Figure 4 *c* reveals that the CB2 protein does not show any direct hydrogen bonding feature with the polar groups of ligands, but shows $\pi$–$\pi$ stacking with residues PHE117 and TRP258. The residues PHE87, VAL113, ILE110, MET265, VLA121 and TYR190 show hydrophobic interaction with JWH-015 ligand inside the binding pocket. Residue ASP189 shows negatively charged interaction towards the ligand. This ligand is also stabilized by the polar group present in the binding pocket of residues like as SER193, THR118, THR114, ASN188, SER285 within the cut-off range of 4 Å. This ligand binds to the CB2 receptor roughly 30 times more strongly when compared with the CB1 receptor (ref. 58). The synthetic drug we docked in the CB receptors was UR-114. This ligand also shows interactive behaviour and is stabilized when perfectly docked in the binding pocket of the CB1 and CB2 receptors. The docking score was –10.63 and –9.384 k cal/mol respectively for CB1 and CB2 receptor. This reduction in the docking score compared to the earlier three ligands is due to the structure of the drug as it contains a substituted cyclopropane ring. In CB1, this ligand shows direct hydrogen-bond interaction with the side chain of the TRP279 residue of the receptor (Figure 3 *d*). The ligand experiences hydrophobic interactions with residues PHE278, ILE290, LEU286, PHE200, PHE174, PHE177, CYS386, VAL196, ALA162 and VAL291. There is also a charged interaction between the ligand and residue ASP163. The $\pi$–$\pi$ stacking is shown by residue PHE170 with the docked ligand. Residues THR197, THR201, SER199 and SER383 show polar interaction with the docked ligand. They show higher affinity towards CB2, but roughly 85 times weaker affinity towards receptor[59].

Figure 4 *d* reveals that UR-144 shows only $\pi$–$\pi$ interaction with the nearby residues like PHE87 and TRP 258. There is a signature of hydrophobic interaction with the surrounding residues like ILE 110, PRO, 178, PHE87, ALA88, PHE117, VAL113 and VAL86. This ligand also

shows polar interaction with residues THR114, THR116, SER285 and ASN188 within the range of 4 Å. Negatively and positively charged residues like ASP189 and LYS109 also play key role in stabilizing this ligand into the binding pocket of the CB2 receptor.

Table 2 shows the docking results and glide e-model. To strengthen our results from IFD, we also performed molecular dynamics simulation using DESMOND[50].

### *Simulation results*

We performed molecular dynamics simulations using DESMOND module of Schrödinger, which initiates with the best-docked ligand into the protein. The stability of the docked ligand inside the protein has been verified by the simulation. We computed the protein–ligand RMSD to measure the average fluctuation in the selection of atoms for a frame with respect to the first frame (reference frame).

RMSD can be formulated for frame $x$ as follows

$$\mathrm{RMSD}_x = \sqrt{\frac{1}{N}\sum_{i=1}^{N}(r_i(t_x)) - (r_i(t_{\mathrm{ref}}))^2}, \quad (1)$$

where $N$ is the number of chosen atoms, $t_{\mathrm{ref}}$ corresponds to the reference time and is generally set to 0 for the first frame and $r_i$ is the position of the selected atoms belonging to frame $x$ recorded at time $t_x$. To calculate RMSD, this procedure was repeated for every frame along the simulation trajectory.

Figure 5 shows the protein–ligand RMSD for all the four ligands with both the CB1 and CB2 receptors. Walking along the $x$-axis gives us an indication about the stability of the ligand with respect to the protein in its binding pocket. The figure shows that the ligand which binds to the protein first aligns along the protein backbone and remains there for rest of the time. Here we present results based on 100 ns simulation trajectory. This simulation length is good enough to explain the stability of the ligand inside the binding pocket of the protein. We can conclude from Figure 5 that the observed values for the ligands are lower than those of the protein that makes the ligand stable inside the pocket; otherwise larger RMSD values for ligand will allow it to diffuse from its initial binding site. For AM-1221 with CB1 and CB2 receptors (Figure 5 *a* and *b*), the average fluctuation in RMSD of protein and ligand averaged between 4.0–5.0 Å and 2.6–3.6 Å (Figure 5 *a* and *b* respectively). Fluctuations within the range 1–3 Å are acceptable for a considerable number of small and globular proteins.

The above results show that the simulation is well-converged and fluctuating along the average value for both protein and ligands. The results of protein–ligand RMSD for ligand AM-2232 with CB1 and CB2 receptors demonstrate the well-converged structure of the ligand inside the binding pocket of protein docked initially along the 100 ns simulation trajectory (Figure 5 *c* and *d* respectively). The average fluctuation of protein and ligand is 4.25–4.75 Å and 1.0–2.0 Å respectively. The overall simulation results show that the ligand is stable at the same place where it was initially docked at the beginning of the simulation. We also examined the protein–ligand RMSD data for ligands JWH-015 and UR-144. Figure 5 *e–h* represents the ligand–protein RMSD plot of JWH-015 and UR-144 into CB1 and CB2. Here too we observed similar trend in the behaviour of deviation as for the other two cases. The average fluctuation of protein and ligand was 4.0–5.0 Å and 4.6–5.6 Å respectively for UR-144. The average fluctuation of protein and ligand was 4.0–5.0 Å and 2.7–4.2 Å respectively for JWH015.

Another important property that deals with the structural stability of the protein is RMSF. This is useful in

**Table 2.** Induced fit docking (IFD) results (k cal/mol) and glide-emodel of the four ligands with cannabinoid type-1 (CB1) and CB2 receptors

| | Docking score (kcal/mol) | | Glide e-model | |
|---|---|---|---|---|
| Ligands | CB1 | CB2 | CB1 | CB2 |
| AM-1221 | –13.48 | –12.73 | –112.02 | –102.36 |
| AM-2232 | –12.38 | –11.05 | –101.22 | –91.37 |
| JWH-015 | –11.86 | –10.75 | –89.35 | –80.61 |
| UR-144 | –10.63 | –09.38 | –77.21 | –66.10 |

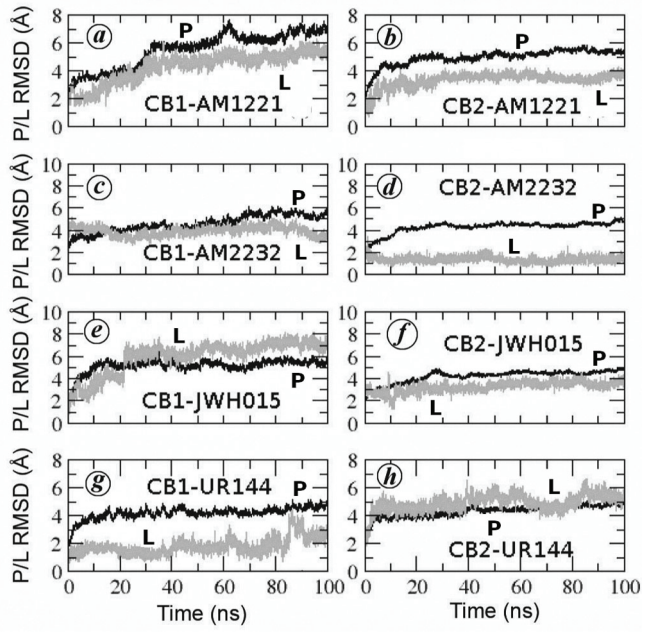


**Figure 5.** Protein–ligand root mean square deviation (RMSD) for ligands (***a***) AM-1221, (***c***) AM-2232, (***e***) JWH-015 and (***g***) UR-144 with CB1, and ligands (***b***) AM-1221, (***d***) AM-2232, (***f***) JWH-015 and (***h***) UR-144 with CB2. The protein curve is marked as P, and ligand curve is marked with L.

characterizing the local structural changes that occur in the protein during simulation. It is formulated as

$$\mathrm{RMSF}_i = \sqrt{\frac{1}{T}\sum_{t=1}^{T}\langle (r_i(t)) - (r_i(t_{\mathrm{ref}}))^2 \rangle}, \quad (2)$$

where $t$ is the trajectory time over which RMSF is calculated, $t_{\mathrm{ref}}$ the time, $r_i$ the position of residue $i$ and the angular bracket denotes the average over the selection of atoms in the residue.

In the RMSF plot, the peak indicates those proteins that fluctuate during the simulations. Lower fluctuation can be directly correlated with the ligand-binding site inside the binding pocket. Figure 6 *a* and *b* shows that the tails of the protein fluctuates more than any other part of the protein (CB1 and CB2 receptors). Usually rigid elements like alpha helix and beta strands fluctuate less as they are more structured compared with the loop regions. The ligand which interacts with the protein makes it stable and does not allow it to fluctuate much when compared with the free moiety. We can also explain the fluctuation in ligand and protein by computing the ligand-RMSF and protein-RMSF respectively. It is also an important quantity which gives a clear view of how individual ligand fragments interact with the receptor protein. This fluctuation shows the entropic role of binding between the ligand and the receptor. The function comes into play once the protein–ligand complex is aligned on the protein backbone and then the ligand RMSF is measured on the ligand heavy atoms (figure not shown). We found that ligands AM-1221 and AM-2232 are more flexible when compared to UR-144 and JWH-015. It explains how the ligand interacts inside the binding pocket of receptor. AM-1221 interacts with more strength with the CB2 receptor and shows greater stability over the other ligands. This can also be explained based on their CB2 activity and corresponding docking scores.

Furthermore, the contacts between ligand and protein can be more specifically explored on the basis of their interactions or contacts as these interactions fluctuate during the course of simulations. The interactions are subdivided into four categories, namely hydrogen bond, hydrophobic, ionic and water bridge. Hydrogen bonding plays a significant role in drug design as it has a strong impact on drug specificity, metabolization and adsorption. The geometric criteria for protein–ligand hydrogen bonds are a distance of 2.5 Å between donor and acceptor atoms (D–H–A), a donor angle of ≥ 120° between the donor hydrogen–acceptor atoms (D–H···A), and an acceptor angle of ≥90° between the acceptor hydrogen-bonded donor atoms (H···A–X). Hydrogen bonding is further subcategorized into backbone acceptor; backbone donor, side-chain acceptor and side-chain donor. The ligand experiences hydrophobic interactions with nearby protein residues, mainly by $\pi$-cation, $\pi$–$\pi$ stacking or other interactions. The geometric criterion for hydrophobic interactions for $\pi$-cation–aromatic and charged groups falls within 4.5 Å; for $\pi$–$\pi$ interaction, two aromatic groups must be stacked face-to-face or face-to-edge. Other interactions between ligands aromatic/aliphatic carbons with nearby residues are primarily due to hydrophobic side chain interaction within 3.6 Å. Figure 7 shows the interaction diagram of the ligands with CB2 along the simulation trajectory. For ligand AM-1221 in CB2, ASN188 makes a H-bond through the side chain with 7.0% probability. Residues ALA83, PHE87, PHE94, VAL113, PHE117, PRO178, TRP258, VAL261, MET265, PHE281, CYS288 and LEU289 show hydrophobic interaction with strength ranging from 5% to 75%. Residues (% strength) PHE281 (32%), TRP258 (4%), PHE97 (7%), PHE94 (7%) and PHE91 (12%) show profound $\pi$–$\pi$ stacking. LYC103 (4%) and PHE117 (2%) show some signature of $\pi$-cation interaction. LYC103 is also involved in the ionic interaction with the ligand. Water molecules present in the system make 'bridge' between the ligand and amino acids, either through donor or acceptor mechanism. THR114, VAL164 and SER193 act as hydrogen-bond acceptors while LYS103 acts as a hydrogen-bond donor. Amino acids ASN188 and ASP189 are categorized as both acceptor and donor moieties. For the AM-2232 ligand, ASN188 forms a H-bond through the side chain with 9.0% probability. Amino acids PHE87, ILE110, VAL113, PHE117, TYR190, TRP 194, ILE198, VAL261, MET265 and CYS288 show hydrophobic interaction and amino acids (% strength) PHE87 (44%), PHE117(37%) and TYR190 (6%) are involved in $\pi$–$\pi$ stacking with the ligand.

No ionic interaction was detected throughout the simulation. The only interaction present is the acceptor type water bridge among amino acids ASN188, SER193 and SER285 with ligand. Only residue ASN188 showed donor behaviour. For ligand JWH-015, amino acids THR114, TRP194 and CYS284 formed weak side chain hydrogen

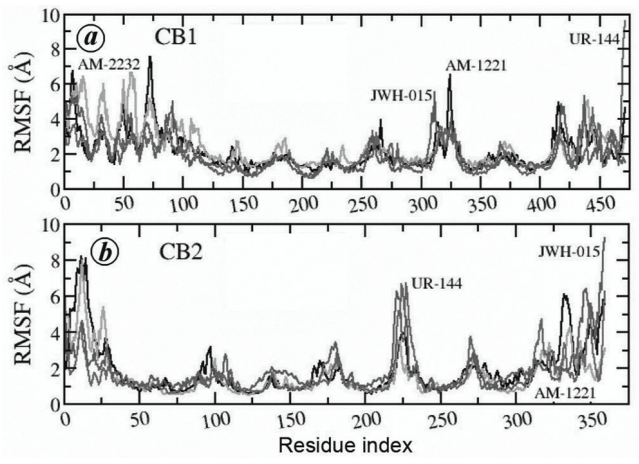


**Figure 6.** Protein–ligand root mean square fluctuation (RMSF) of AM-1221, AM-2232, JWH-015, and UR-144 with (***a***) CB1 and (***b***) CB2 receptors respectively.

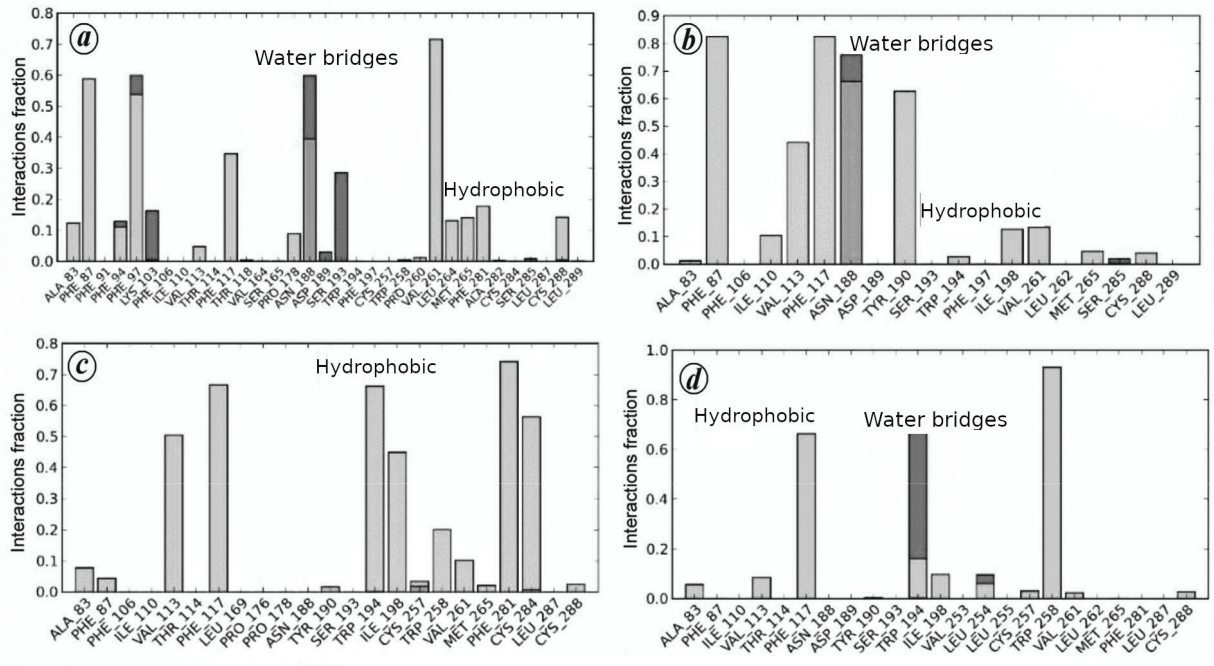


**Figure 7.** Interaction diagram of CB2 with (***a***) AM-1221, (***b***) AM-2232, (***c***) JWH-015 and (***d***) UR-144.

bonds of strength less than 2%. The amino acid residues PHE87, ILE110, VAL113, PHE117, TRP194, ILE198, TRP258, VAL261, PHE281 and CYS284 show only hydrophobic interactions with the ligand present inside the binding pocket of the protein. Residues PHE87, PHE117, TRP194, TRP258 and PHE281 showed $\pi$–$\pi$ stacking with strength 2–37%. There was no ionic or water-bridge contact between the ligand and amino acid residues. Amino acid THR114 formed side-chain hydrogen bond with ligand UR-144, with 21% in strength. The interaction types and fractions are shown for the interacting amino acids throughout the course of the molecular dynamics simulations. Residues ALA83 PHE87, VAL113, PHE117, TRP194, ILE198 and TRP258 showed hydrophobic contact, whereas residues PHE117 and TRP258 showed $\pi$–$\pi$ stacking with percentage strength of 18% and 54% respectively. No ionic interaction was reported in this case. Residues ASN188, ASP189 and LEU254 showed acceptor behaviour in the water bridge whereas THR114 and TRP194 showed donor behaviour. In the present study, we restrict our explanation only to CB2, although Figure 8 shows the protein–ligand RMSD for all the four ligands with the CB1 receptor.

The stability of the ligands inside the protein binding pocket can also be explained based on the interaction energy between the ligands and the protein. The potential energy of the system (protein + ligand + water) is given by

$$E_{\text{total}} = E_{\text{Col}} + E_{\text{vd}W} + E_{\text{bond}} + E_{\text{angle}} + E_{\text{torsion}}. \quad (3)$$

Electrostatic interactions are mainly classified into charge–charge, charge–dipole and dipole–dipole interactions between the ligand and protein binding site. The charge–charge interactions arise between oppositely positively or negatively charged atoms, ligand functional groups or protein side chains. The interactions between ionized amino acid side chains and the dipole of the ligand moiety also contribute towards the enthalpy change associated with binding due to charge–dipole interaction. Dipole moment from the polar side chain of amino acids influences the ligand–protein interaction. Binding is also influenced by the van der Waals interaction and is important to elucidate the structure and interaction of biological species. We used the simulation event analysis tool from DESMOND to estimate the binding energy due to non-bonded interaction between a ligand and binding site of the protein. Based on the calculated binding energy, ligand AM-1221 shows total interaction energy of –58.64 kcal/mol, which makes it quite stable in the pocket. Ligands AM-2232, UR-144 and JWH-015 show binding energy of –55.77, –48.53 and –48.25 k cal/mol respectively.

## Conclusion

We used multiple template comparative homology modelling algorithm to construct a 3D model for the CB2 receptor. We performed docking and molecular dynamics simulation study of four synthetic drugs in both the CB1 and CB2 receptors. Our docking and simulation results show better affinity of the ligands towards CB receptors, and they are reasonably stable inside the binding pocket. Ligand AM-1221 shows the highest binding affinity (–12.73 k cal/mol), whereas UR-144 shows the lowest

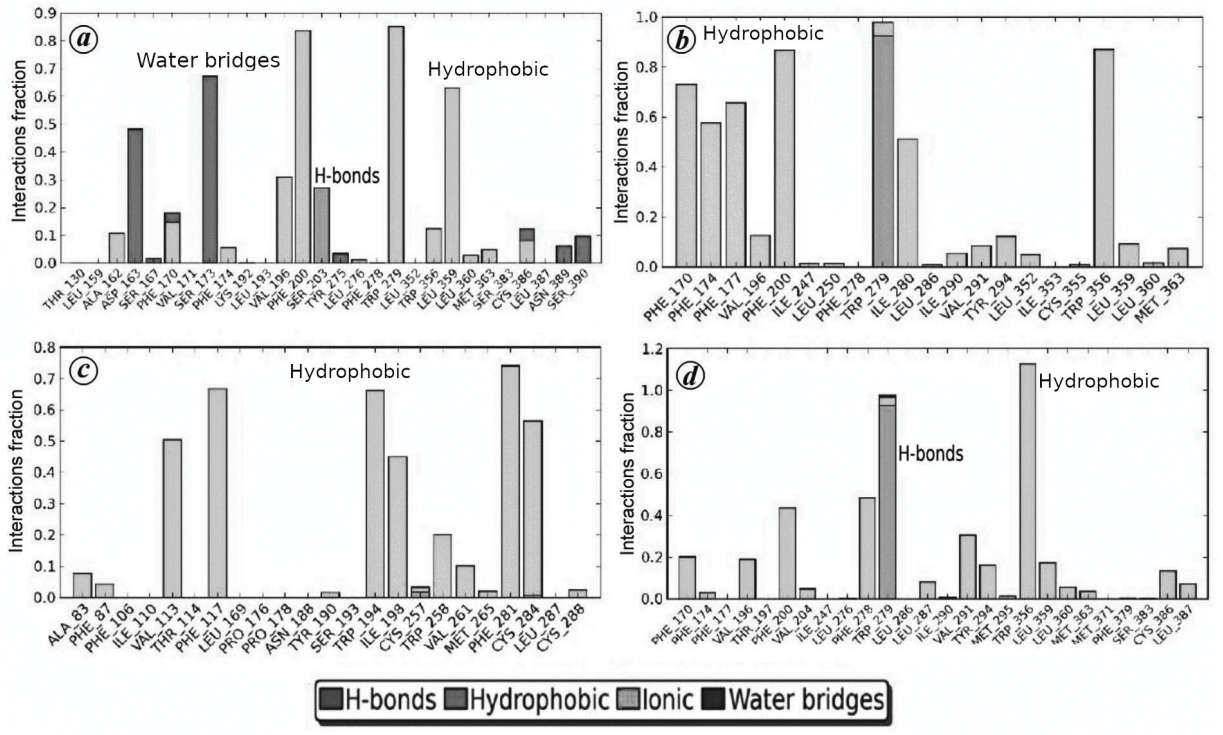


**Figure 8.** Interaction diagram of CB1 with (***a***) AM-1221, (***b***) AM-2232, (***c***) JWH-015 and (***d***) UR-144.

(–9.83 k cal/mol) towards the CB2 receptor. Molecular properties of the ligands, including molecular, polar and solvent accessible surface areas and intramolecular hydrogen bonds were evaluated throughout the course of molecular dynamics simulations, which also support the agonist activity of the ligands towards the CB2 receptor. The computed results should be helpful to design the ligands with distinct pharmacological properties associated with the CB2 receptor.


1. Edery, H., Grunfeld, Y., Ben-Zvi, Z. and Mechoulam, R., Structural requirements for cannabinoid activity. *Ann. N.Y. Acad. Sci*., 1971, **191**, 40–53.
2. Gaoni, Y. and Mechoulam, R., Isolation, structure and partial synthesis of an active constituent of hashish. *J. Am. Chem. Soc.*, 1964, **86**, 1646–1647.
3. Martin, B. R., Balster, R. L., Razdan, R. K., Harris, L. S. and Dewey, W. L., Behavioral comparisons of the stereoisomers of tetrahydrocannabinols. *Life Sci.*, 1981, **29**, 565–574.
4. Lambert, D. M. and Fowler, C. J., The endocannabinoid system: drug targets, lead compounds and potential therapeutic applications. *J. Med. Chem*., 2005, **48**(16), 5059–5087.
5. Pertwee, R. (ed.), *Cannabinoids*, Springer-Verlag, 2005, p. 2.
6. Galiegue, S. *et al.*, Expression of central and peripheral cannabinoid receptors in human immune tissues and leukocyte subpopulations. *Eur. J. Biochem.*, 1995, **232**(1), 54–61.
7. Hanson, M. A. *et al.*, Crystal structure of a lipid G protein-coupled receptor. *Science*, 2012, **335**, 851–855.
8. Wu, H. *et al.*, Structure of the human-opioid receptor in complex with JDTic. *Nature*, 2012, **485**, 327–332.
9. Manglik, A. *et al.*, Crystal structure of the micro-opioid receptor bound to a morphinan antagonist. *Nature*, 2012, **485**, 321–326.
10. Wang, C. *et al.*, Structural basis for molecular recognition at serotonin receptors. *Science*, 2013, **340**, 610–614.
11. Pacher, P. and Mechoulam, R., Is lipid signaling through cannabinoid 2 receptors part of a protective system? *Prog. Lipid Res.*, 2011, **50**(2), 193–211.
12. Ashton, J. C. *et al*., Cannabinoid CB1 and CB2 receptor ligand specificity and the development of CB2-selective agonist. *Curr. Med. Chem*., 2008, **15**, 1428–1443.
13. Huffman, J. W. and Marriott, K. S. C., Recent advances in the development of selective ligands for the cannabinoid CB2 receptor. *Curr. Top. Med. Chem.*, 2008, **8**, 187–204.
14. Benito, C. *et al*., Cannabinoid CB2 receptors and fatty acid amide hydrolase are selectively overexpressed in neuritic plaque-associated glia in Alzheimer's disease brains. *J. Neurosci.*, 2003, **23**(35), 11136–11141.
15. Fernandez-Ruiz, J., Pazos, M. R., García-Arencibia, M., Sagredo, O. and Ramos, J. A., Role of CB2 receptors in neuroprotective effects of cannabinoids. *Mol. Cell. Endocrinol.*, 2008, **286**, S91–S96.
16. Tolon, R. M. *et al.*, The activation of cannabinoid CB2 receptors stimulates *in situ* and *in vitro* beta-amyloid removal by human macrophages. *Brain Res.*, 2009, **1283**(11), 148–154.
17. Tabrizi, M. A., Baraldi, P. G., Borea, P. A. and Varani, K., Medicinal chemistry, pharmacology and potential therapeutic benefits of cannabinoid CB2 receptor agonist. *Chem. Rev*., 2016, **116**, 519–560.
18. Baraldi, P. G. *et al.*, 7-oxo-[1,4]oxazino[2,3,4-Ij]quinoline-6-carboxamides as selective CB(2) cannabinoid receptor ligands: structural investigations around a novel class of full agonists. *J. Med. Chem.*, 2012, **55**(14), 6608–6623.
19. Aghazadeh, T. M. *et al.*, Design, synthesis and pharmacological properties of new heteroarylpyri-dine/heteroarylpyrimidine derivatives as CB(2) cannabinoid receptor partial agonists. *J. Med. Chem*., 2013, **56**(3), 1098–1112.
20. Aghazadeh, T. M. *et al.*, Discovery of 7-oxopyrazolo[1,5-A]pyrimidine-6-carboxamides as potent and selective CB(2) cannabinoid

receptor inverse agonists. *J. Med. Chem.*, 2013, **56**(11), 4482–4496.
21. Ibrahim, M. M. *et al.*, Activation of CB2 cannabinoid receptors by AM1241 inhibits experimental neuropathic pain: pain inhibition by receptors not present in the CNS. *Proc. Natl. Acad. Sci. USA*, 2003, **100**, 10529–10533.
22. Valenzano, K. J. *et al.*, Pharmacological and pharmacokinetic characterization of the cannabinoid receptor 2 agonist, GW405833, utilizing rodent models of acute and chronic pain, anxiety, ataxia and catalepsy. *Neuropharmacology*, 2005, **48**, 658–672.
23. Rice, A. S., Farquhar-Smith, W. P. and Nagy, I., Endocannabinoids and pain: spinal and peripheral analgesia in inflammation and neuropathy. *Prostaglandins Leukot. Essent. Fatty Acids*, 2002, **66**, 243–256.
24. Richardson, J. D., Aanonsen, L. and Hargreaves, K. M. Antihyperalgesic effects of spinal cannabinoids. *Eur. J. Pharmacol*., 1998, **345**, 145–153.
25. http://www.hhs.gov/ash/oah/adolescent-health-topics/substance-abuse/illicit-and-non-drug-use.html
26. Fernandez-Ruiz, J., Pazos, M. R., García-Arencibia, M., Sagredo, O. and Ramos, J. A., Role of CB2 receptor in neuroprotective effects of cannabinoids. *Mol. Cell. Endocrinol.*, 2008, **286**, S91.
27. Makriyannis, A. and Deng, H., Cannabimimetic indole derivatives, granted 2001-06-07.
28. Makriyannis, A. and Deng, H., Cannabimimetic indole derivatives, granted 2007-07-10.
29. Murataeva, N., Mackie, K. and Straiker, A., The CB2-preferring agonist JWH-015 also potently and efficaciously activates CB1 in autaptic hippocampal neurons. *Pharmacol. Res*., 2012, **66**(5), 437–442.
30. Poso, A. and Huffman, J. W., Targeting the cannabinoid CB2 receptor: modelling and structural determinants of CB2 selective ligands. *Br. J. Pharmacol.*, 2008, **153**(2), 335–346.
31. Jacobson, M. P. *et al.*, A hierarchical approach to all-atom protein loop prediction. *Proteins: Struct., Funct. Bioinformat.*, 2004, **55**, 351–367.
32. Jacobson, M. P., Friesner, R. A., Xiang, Z. and Honig, B., On the role of the crystal environment in determining protein side-chain conformations. *J. Mol. Biol.*, 2002, **320**, 597–608.
33. Schrödinger Release 2015-3: Prime, version 4.1, Schrödinger, LLC, New York, USA, 2015.
34. Zhu, K. *et al.*, Antibody structure determination using a combination of homology modeling, energy-based refinement, and loop prediction. *Prot.: Struct., Funct. Bioinformat.*, 2014, **82**, 1646–1655.
35. Salam, N. K., Adzhigirey, M., Sherman, W. and Pearlman, D. A., Structure-based approach to the prediction of disulfide bonds in proteins. *Prot. Eng. Design Select.*, 2014, **27**, 365–374.
36. Beard, H., Cholleti, A., Pearlman, D., Sherman, W. and Loving, K. A., Applying physics-based scoring to calculate free energies of binding for single amino acid mutations in protein-protein complexes. *PLoS ONE*, 2013, **8**, e82849.
37. Biologics Suite 2015-3: BioLuminate, version 2.0, Schrödinger, LLC, New York, USA, 2015.
38. Protein Data Bank, repository; http://www.rcsb.org
39. Warne, T. *et al*., The structural basis for agonist and partial agonist action on a [bgr] 1-adrenergic receptor. *Nature*, 2011, **469**, 241–244.
40. Hua, T. *et al*., Crystal structure of the human cannabinoid receptor CB1. *Cell*, 2016, **167**, 750–762.
41. Sastry, G. M. *et al.*, Protein and ligand preparation: parameters, protocols, and influence on virtual screening enrichments. *J. Comput-Aided Mol. Des.*, 2013, **27**, 221–234.
42. Schrödinger Suite 2015-3 protein preparation wizard; Epik version 3.3, Schröidinger, LLC, New York, USA, 2015; Impact version 6.8, Schrödinger, LLC, New York, USA, 2015; Prime version 4.1, Schrödinger, LLC, New York, USA, 2015.
43. LigPrep, version 3.5, Schrödinger, LLC, New York, USA, 2015.
44. Farid, R., Day, T., Friesner, R. A. and Pearlstein, R. A., New insights about HERG lockade obtained from protein modeling, potential energy mapping, and docking studies. *Bioor. Med. Chem.*, 2006, **14**, 3160–3173.
45. Schrödinger Suite 2015-3 induced fit docking protocol; Glide version 6.8, Schrödinger, LLC, New York, USA, 2015; Prime version 4.1, Schrödinger, LLC, New York, USA, 2015.
46. Osman, A. G. *et al*., Bioactive products from singlet oxygen photooxygenation of cannabinoids. *Eur. J. Med. Chem.*, 2018, **143**, 983–996.
47. Friesner, R. A. *et al.*, Extra precision glide: docking and scoring incorporating a model of hydrophobic enclosure for protein–ligand complexes. *J. Med. Chem.*, 2006, **49**, 6177–6196.
48. Bowers, K. J. *et al.*, Scalable algorithms for molecular dynamics simulations on commodity clusters. In SC'06: Proceedings of the 2006 ACM/IEEE Conference on Supercomputing, 2006, p 43; doi:10.1109/SC.2006.54.
49. Shivakumar, D. *et al.*, Prediction of absolute solvation free energies using molecular dynamics free energy perturbation and the OPLS force field. *J. Chem. Theory Comput.*, 2010, **6**, 1509–1519.
50. Desmond Molecular Dynamics System, version 4.3, D. E. Shaw Research, New York, USA, 2015; Maestro-Desmond Interoperability Tools, version 4.3, Schrödinger, New York, USA, 2015.
51. Guo, Z. *et al.*, Probing the $\alpha$-helical structural stability of stapled p53 peptides: molecular dynamics simulations and analysis. *Chem. Biol. Drug Des.*, 2010, **75**, 348–359.
52. Tuckerman, M. E. and Berne, B. J., Molecular dynamics algorithm for multiple timescales: systems with disparate masses. *J. Chem. Phys*., 1991, **94**, 1465.
53. Martyna, G. J., Klein, M. L. and Tuckerman, M. E., Nose–Hoover chains: the canocial ensemble via continuous dynamics. *J. Chem. Phys*., 1992, **97**, 2635.
54. Martyna, G. J., Tobias, D. J. and Klein, M. L., Constant pressure molecular dynamics algorithms. *J. Chem. Phys*., 1994, **101**, 4177–4189.
55. Cavasotto, C. N. and Phatak, S. S., Homology modeling in drug discovery: current trends and applications. *Drug Discov. Today*, 2009, **14**, 676–683.
56. Dhopeshwarkar, A. and Mackie, K., CB2 cannabinoid receptors as a therapeutic target – what does the future hold? *Mol. Pharmacol*., 2014, **86**(4), 430–437.
57. Malan, P. T. *et al*., CB2 cannabinoid receptor-mediated peripheral antinociception. *Pain*, 2001, **93**, 239–245.
58. Aung, M. M. *et al.*, Influence of the *N*-1 alkyl chain length of cannabimimetic indoles upon CB1 and CB2 receptor binding. *Drug Alcohol Depend*, 2000, **60**(2), 133–140.
59. Frost, J. M. *et al.*, Indol-3-ylcycloalkyl ketones: effects of *N*-1 substituted indole side chain variations on CB2 cannabinoid receptor activity. *J. Med. Chem.*, 2010, **53**(1), 295–315.

ACKNOWLEDGEMENTS. I thank the Science and Engineering Research Board, Department of Science and Technology, Government of India for the National Post-Doctoral Fellowship (Grant PDF/2019/001240). I also thank Dr Khaled. M. Elokely for help in the initial set-up of the systems and Prof. Michael L. Klein for valuable discussions. Part of the calculations was carried out at the High-Performance Computing Facility (OwlsNest) of Temple University, Philadelphia, USA.

Received 22 August 2021; revised accepted 23 November 2021

doi: 10.18520/cs/v122/i2/167-177